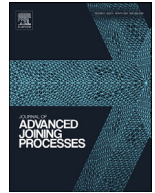




ELSEVIER

Contents lists available at ScienceDirect

Journal of Advanced Joining Processes

journal homepage: www.elsevier.com/locate/jajp

Influence of the process parameter of resistance spot welding and the geometry of weldable load introducing elements for FRP/metal joints on the heat input

Sven Roth*, Alisa Hezler, Oliver Pampus, Sven Coutandin, Jürgen Fleischer

wbk Institute of Production Science, Karlsruhe Institute of Technology (KIT) Kaiserstraße 12, 76131 Karlsruhe, Germany

ARTICLE INFO

Keywords:

Resistance spot welding
Composites
CFRP
Heat input
Joining
Inserts

ABSTRACT

Resistance spot welding is one of the most economical joining processes when manufacturing conventional steel bodies in the automotive sector. However, its applicability in future body constructions is limited due to the growing material mix. Since the demands of efficiency and weight reduction are steadily increasing, modern car bodies implement lightweight materials, especially fibre-reinforced plastics (FRP), in a multi-material design. To enable the joining of FRP/steel constructions with resistance spot welding, weldable inserts can be embedded in the FRP. In order to evaluate the thermal damage to the surrounding polymer, an experimental study of the welding induced heat is presented in this study. The influence of welding parameter, metal sheet thickness and alloying degree on the heat input are characterised. Based on this data, weldability lobes and energy input diagrams are derived. Furthermore, the dependency between insert geometry and the resulting temperature distribution is examined.

Introduction

Resistance spot welding is considered the preferred and most significant joining method for steel-intensive car body construction in the automotive industry and shows a high degree of automation (Pepke, 2014). For dissimilar steel/FRP joints in multi-material designs, alternative joining techniques have so far been used (Meschut et al., 2014). In addition to adhesive bonding, the focus of research and technology is on semi-tubular and full punch riveting (Friedrich, 2017; Lehmingner and Wagner, 2015), joining with flow drill screws or thread forming screws (Wilhelm, 2016), clinching (He, 2017) or the modified blind riveting process according to (Podlesak, 2017). However, these methods are not only more cost-intensive but are also damaging the composite structure and thus weakening the joint.

Great potential for joining dissimilar FRP/steel connections by means of resistance spot welding can be seen in metallic force-introducing elements that are integrated in the fibre composite (inserts). These inserts can either be integrated into the material composite in a fibre-damaging way after part production (Bhavesh et al., 2010; Holtzsche and Jüttner, 2017) or in a fibre-conform way (Jansen and Kunze, 2016; Ruffing and Baron, 2019; Roth et al., 2019, 2020) during part production, serving as the interface for spot welding to other steel components.

For example in the resin-transfer moulding process, the insert is first positioned between the stacks of the preformed plies, which are then infiltrated using a purpose-made mould. In addition to the form-fit bonding of the two components, the curing of the resin system leads to an adhesive bond between the FRP and the metal (so-called "co-cured bonding") (Gebhardt et al., 2018). The bonding strength is sufficient for typical spot weld requirements (Ruffing and Baron, 2019) and can be further increased by specific surface pre-treatments (Gebhardt et al., 2018).

Given the widespread industrial use of resistance spot welding in the field of steel/steel joints, also dissimilar FRP/steel joints could be realised on already existing production lines for industrial applications. For a transfer into series applications, however, precise knowledge of the temperatures within the fibre composite during spot welding is essential because even a short disposition at temperatures between 230 °C and 300 °C causes permanent damage (Visakh and Arao, 2015; Natarajan and Murugavel, 2017).

The temperature peaks occurring in the composite are again determined by the temperature distribution of the embedded inserts. But due to the characteristic geometry of spot weldable inserts (Fig. 1), the mapping of the temperature distribution during the welding process represents a major challenge.

The occurring temperatures are decisively determined by the heat input accompanying spot welding. The main influencing factors are pa-

* Corresponding author.

E-mail address: sven.roth@kit.edu (S. Roth).



Fig. 1. Schematic illustration of the welded FRP/metal connection (Roth et al., 2019).

parameters such as welding current, welding time, electrode force and the material properties of the parts to be joined. Basic cause-effect relationships between the individual parameters during the welding process were investigated by Dickinson et al. (1980). First models of the heat distribution during welding and the forming of the nugget diameter have already been introduced by Cho and Cho (1989). A model adjustment was made by estimating the temperature distribution during the welding process via the microstructure formation. The influence of the process parameters on the heat input with varying welding current is examined by Hayat (2011) and with varying welding time by Kocabekir et al. (2008). However, the question which combinations of welding current and welding time at a certain required nugget diameter implicate the lowest possible heat input remains unanswered. The reduction of the welding energy input under consideration of a given spot weld quality is not addressed.

Previous investigations of heat distribution during resistance spot welding were mostly carried out using numerical and analytical approaches. Wan et al. (2014) investigated the effect of the welding current on the radial temperature distribution in a component based on a numerical simulation. Mirzaei et al. (2017) modelled the weld joint strength based on the temperature distribution during the welding process. The microstructure in the welding area was described numerically by Lu et al. (2018) and analytically by Sheikhi et al. (2017) based on the temperature distribution in the welding area. Up to now, a research deficit lies in the often missing validation of the simulated temperature distribution by experimentally determined temperatures due to the difficulties of temperature measurement itself.

KIM and Eagar (1989) determined the heat distribution for different electrode thicknesses and cooling water flow rates experimentally by using infrared emission monitoring and cinematography, which however require a corresponding accessibility of the measuring zone. Han et al. (1989) investigated the temperature distribution using metallography and thermocouples. Akkus (2009) used a digital thermometer to measure the influence of sheet thickness and welding current on the cooling rate and temperature distribution in the component. Precise measurement results obtained by using thermocouples require considering the influence of their net mass on the measurement result.

The influence of different materials from car body construction on the spot welding process has already been investigated in detail by DVS/EFB (2016). Plane sample geometries with significantly larger dimensions in length and width compared to the sheet thickness were mostly used in those investigations. Spot welding of smaller samples was considered experimentally and simulatively by Wan et al. (2014), Sheikhi et al. (2017), Chigurupati et al. (2010), Moshayedi and Sattari-Far (2012), and Zhao et al. (2019). The considered aspect ratio of plate thickness to width was always larger than 23.5. The influence of smaller sample dimensions on the welding process is unknown so far. Furthermore, the considered geometries involve only plane samples. The cause-effect relationships between the geometry, the production process of non-planar component geometries and the temperature distribution in the workpiece during the spot-welding process have not been properly investigated until today.

Materials and methods

In this paper, the materials 1.0338 and 1.4301 with a nominal sheet thickness t of 1.25 mm were examined. Both steels are easily weldable and have very different thermal conductivity properties (Smithells et al., 2004). The spot welds were carried out using a Bosch 1000 Hz MFDC

welding current inverter Type PSI 63C0 36KA and a pneumatically controlled robot welding gun made by Düring Schweißtechnik GmbH, see Fig. 2 (left side). The used transducer from Type PSG6130.00 PSTK was manufactured by Bosch and has a maximum output of 130 kVA. According to DIN EN ISO 5821 (Deutsches Institut für Normung e.V., 2010), the welding electrode cap Type G0 was chosen. It has a diameter of 16 mm, a contact diameter of 6.0 mm and can be centred towards the welding specimen by the device shown in Fig. 2 (right side).

Using the BOS6000 software, the voltage and dynamic resistance were recorded at intervals of 1.0 ms during the welding series. The measurement was carried out with the help of the welding control PSI 63C0, an external device was not used. The electrode force was controlled by the WINSPZ KCT CPX program from Festo AG & Co. KG. A force of 3.0 kN was selected for the material 1.0338, whereas 5.0 kN was chosen for the material 1.4301. The investigation of the welding parameter-dependant heat input was carried out on samples with a dimension of $50 \times 50 \text{ mm}^2$. The selected sample size is clearly above the expected heat influence range according to Wan et al. (2014). Weldability lobes were used as a basis, which, according to DIN EN ISO 14,327 (Deutsches Institut für Normung e.V., 2004), were generated from four growth curves each at constant electrode force. The heat input was evaluated by correlation of the spot weld diameter according to DIN EN ISO 10,447 (Deutsches Institut für Normung e.V., 2015) with the actually measured energy input of the BOS6000.

The analysis of the temperature distribution of spot weldable inserts was performed on the sample geometries shown in Fig. 3 (left side). The plane test specimens with the same outer diameter served as joining partners for the deep-drawn inserts. Using four different temperature indicating lacquers, see Fig. 3 (right side), the maximum local temperature occurring during the spot weld was determined with an accuracy of $\pm 1.0\%$ and a response time of 1 ms (OMEGA, 2018; VDI/VDE, 2015). The recording of the lacquer-specific colour change was performed by optical measurement of the samples.

Results

First, the weldability lobes shown in Fig. 4 were created according to the DIN EN ISO 14,327 (Deutsches Institut für Normung e.V., 2004) for the purpose of evaluating the welding parameters with regard to the resulting energy input. To this end, four welding times were selected which, based on the welding time recommended in DIN EN ISO. DIN EN ISO 14373:2015-06 (2020) and Schmitt and GmbH (2015), were decreased by 20 ms each. Pursuant to DIN EN ISO 14,327 (Deutsches Institut für Normung e.V., 2004), a minimum nugget diameter of $3, 5 \cdot \sqrt{t}$ was selected as lower quality limit (left-hand side of the welding area; $I_{S_{min}}$). The upper quality limit (right-hand side of the welding area; $I_{S_{max}}$) on the other hand describes the transition towards the formation of weld spatters. Welding parameters within both quality limits lead to a quality-compliant spot weld.

Fig. 4 shows that material 1.0338 has a significantly wider welding area with considerably higher welding times and welding currents. The welding current range of both materials is constant, except for the welding time of 120 ms of material 1.4301. Furthermore, a tendency of increasing welding current with decreasing welding time can be observed for both materials.

Based on the weldability lobes, the curves of the electrode voltage as well as the dynamic resistance documented by the BOS6000 software, the diagrams shown in Fig. 5 have been created to evaluate the energy input.

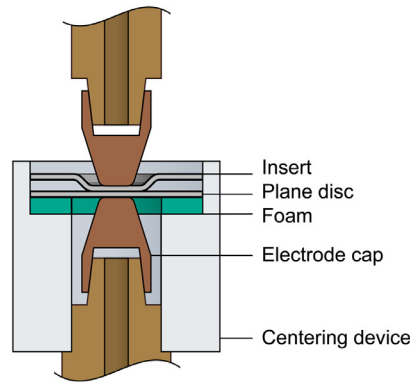
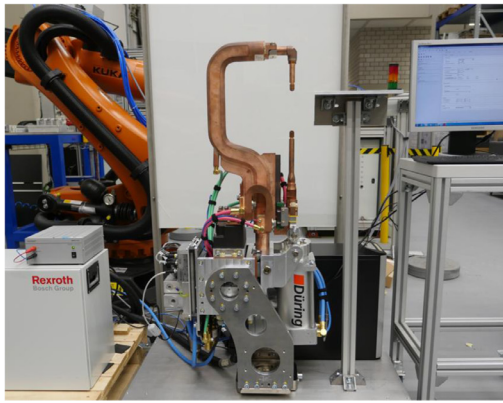


Fig. 2. Experimental setup (left side); centering device (right side).

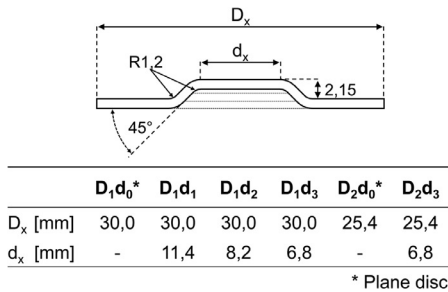


Fig. 3. Geometry of used inserts (left side); preparation with temperature laquers (right side).

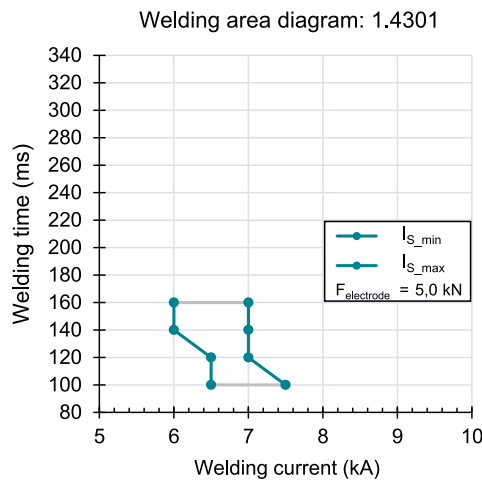
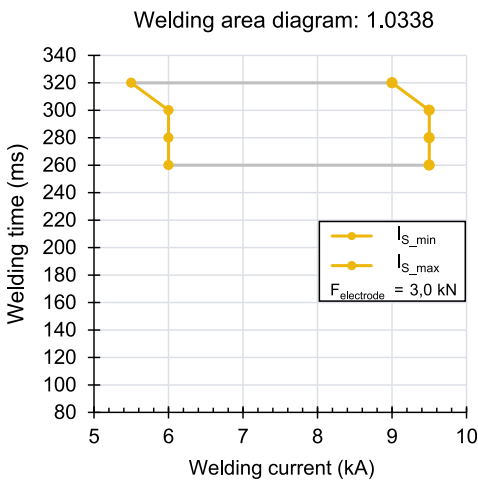


Fig. 4. Experimentally determined weldability lobes for material 1.0338 and 1.4301 ($t = 1.25$ mm).

The filled area in Fig. 5 represents the acceptable welding area (AWR) between lower bound (I_{S_min}) and upper bound (I_{S_max}). Moreover the hatched area represents the inadequate welding range (IWR). For both materials, an increasing energy input with increasing welding lens diameter can be observed. It can also be noted that with the same welding lens diameter a longer welding time leads to a higher energy input. Therefore, it can be assumed that due to the longer welding process, more heat is dissipated from the welding process by heat conduction in the base material. As can already be expected from Fig. 4, there is a clear difference in the energy level of the two materials and a wider range of energy input of material 1.0338 compared to 1.4301. The range is 2890 J for material 1.0338 and 743 J for the austenitic steel 1.4301.

Circular specimens with diameters of 30.0 mm and 25.4 mm of the materials 1.4301 and 1.0338 were examined for the purpose of evaluating the temperature distribution during spot welding with regard to the influencing variables such as insert material and outer diameter. The measuring of local temperatures during spot welding was carried out

with the help of temperature indicating laquers, see Fig. 3 (right side). For the data collection of all four variants, eight samples for each variant were welded and evaluated choosing welding parameters with high energy input.

As illustrated in Fig. 6, the temperature peaks decrease steadily during the welding process with increasing distance from the welding point. Material 1.0338 with its very high thermal conductivity has a much larger heat-affected zone compared to the austenitic steel 1.4301. For example, the isotherm of 149 °C of material 1.0338 with an outer diameter of 30.0 mm is approximately 50.3% further away from the welding centre than the one of 1.4301. Both materials also show a slightly increased heat-affected zone in samples with smaller outer diameter despite identical welding parameters and the same energy input.

Fig. 6 shows the measurement results of material 1.0338 with the previously depicted geometries of Fig. 3. In contrast to the plane specimens, the insert geometries investigated show a less uniform temperature propagation and an increased temperature gradient in the deformed area. With decreasing inner diameter d and constant outer diameter D ,

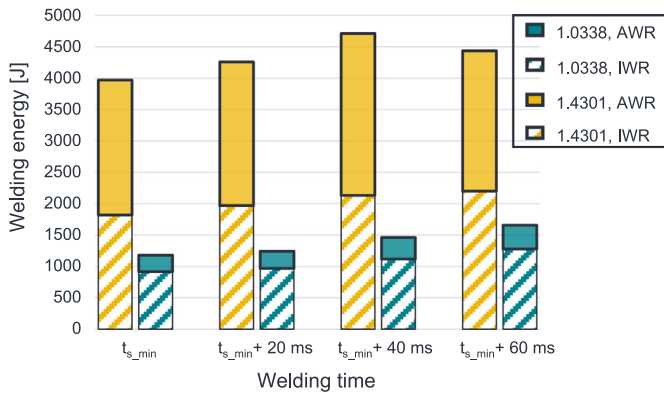


Fig. 5. Comparison of the energy inputs at varying welding parameters.

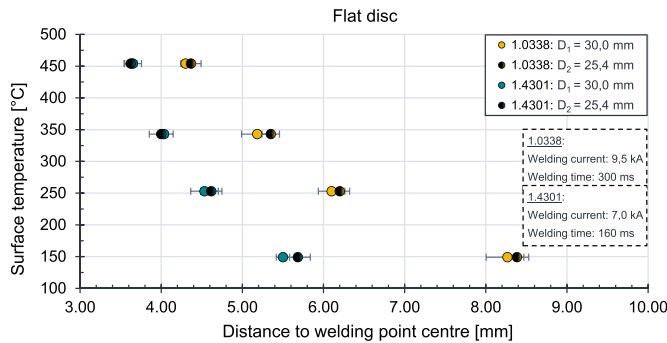


Fig. 6. Temperature distribution during spot welding of plane specimens.

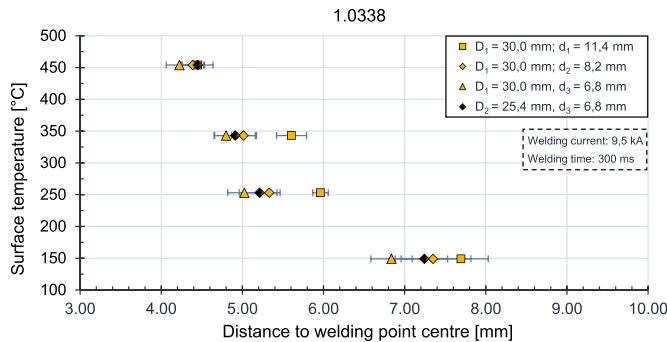


Fig. 7. Temperature distribution during spot welding of 1.0338 with different insert geometries.

a steady reduction of the heat-affected zone can be observed. The radial spread of the maximum temperatures is always lower than the one of the plane samples. With a constant inner diameter and smaller outer diameter, however, an increase in the heat-affected zone can be observed, see D_1d_3 and D_2d_3 . This observation is consistent with those of plane specimens.

The maximum temperatures during spot welding for material 1.4301 are shown in Fig. 8. In agreement with the observations of the samples from material 1.0338 (see Fig. 7), there is also less temperature propagation with decreasing inner diameter. The size of the heat-affected zone is also below the measured values of plane samples. Due to the lower thermal conductivity, the majority of the measuring points lie within the formed area, so that the increased temperature gradient in the transition area can be detected less sharply. Nevertheless, the trend of a larger heat-affected area with decreasing outside diameter can also be seen in austenitic steel.

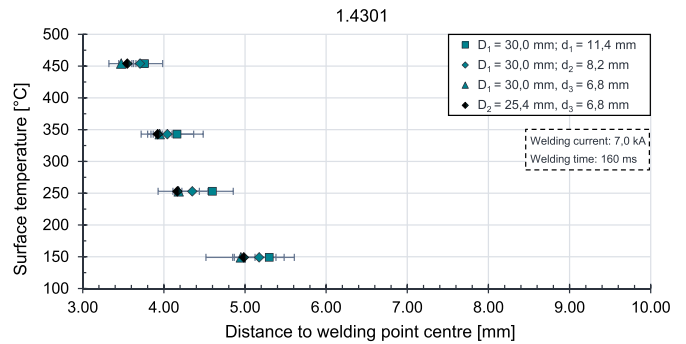


Fig. 8. Temperature distribution during spot welding of 1.4301 with different insert geometries.

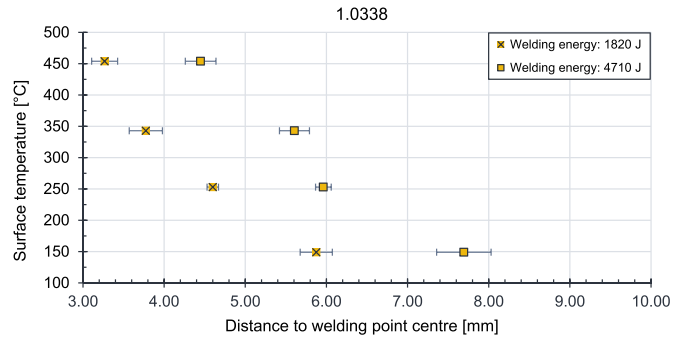


Fig. 9. Temperature distribution of different energy inputs taking the insert geometry D_1d_1 as an example.

Discussion

The measured values of the energy input of all spot welds in Fig. 5 correlate with the expected energy input based on the weldability lobes in Fig. 4. It is noticeable that the increase in the energy required to reach the minimum nugget diameter at higher welding times is different for the two materials. An increase in welding time by 23.1% results in an increased energy requirement of 20.1% for material 1.0338, whereas a comparable energy increase of 21.8% requires a 40.0% increase in welding time for material 1.4301. This means that the formation of the minimum nugget diameter when using longer welding times for material 1.0338 requires a higher increase in energy input than in the case with austenitic steel. This can be explained by the higher thermal conductivity of material 1.0338, by which more heat is dissipated from the welding area during the welding process and is therefore no longer available for forming the spot weld. Furthermore it has to be noted, that the different level of the electrode force are influencing the required energy input and therefore the temperature distribution.

The differences in energy input and thermal conductivity of the investigated materials are also reflected in the observed temperature curves. For example, material 1.0338 shows a much more pronounced heat-affected zone. The observed temperatures of plane samples show a good qualitative agreement with the predictions of Wan et al. (2014) and Chigurupati et al. (2010) but the absolute values differ due to differences in the choice of material and welding parameters.

The fact that the heat-affected zone can be significantly influenced by a suitable choice of welding parameters can be seen in Fig. 9. Eight specimens with a welding current of 6 kA, a welding time of 260 ms and an electrode force of 3 kN were joined exemplarily for the insert geometry D_1d_1 , at which an energy input of 1820 J could be recorded. The affected zone observed here is significantly below the welding parameters used in Fig. 7, which involve an energy input of 4710 J. For a damage-free joining of FRP/metal joints by means of weldable inserts,

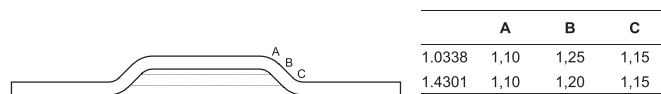


Fig. 10. Material thickness in the forming area using the example of insert geometry $D_1 d_1$ (in mm).

it is therefore advisable to choose the welding parameters with the lowest possible energy input. Therefore, short welding times are to be preferred.

When observing the temperature curves of the insert geometries examined, further conclusions can be drawn. For one thing, it shows that a decrease in sample size from 30.0 mm to 25.4 mm leads to a larger heat-affected zone. This behaviour can also be observed for plane samples and can be explained by a reduced heat dissipation into the peripheral area. Due to the smaller sample width to sheet thickness ratio of 20.3, the heat dissipation capacity into the peripheral area of the inserts is limited causing the isotherms to shift to the peripheral area.

For another thing, all formed insert variants show an increasingly small heat affected zone with decreasing diameter d . This can be explained on the one hand by a locally reduced thermal conductivity (Chu and Ho, 1978) and on the other hand by a thinning of the sheet thickness as a result of the deep drawing process. To support the hypothesis of material thinning, microsection samples were prepared and the local sheet thickness measured microscopically at the measuring points marked in Fig. 10. For both materials, a reduction in sheet thickness of about 12% and 8% respectively can be observed in area A and C. It can therefore be concluded that the material cross section available for heat dissipation is reduced in the formed area and consequently, a lower thermal output occurs in insert areas outside the forming area.

Conclusion

The influence of welding parameters and insert geometry on the formation of local temperature peaks was investigated in the context of using weldable inserts for damage-free joining of fibre-reinforced plastics to metal structures. The following conclusions can be drawn:

1. To achieve the required nugget diameter, short welding times at higher welding currents result in a lower heat input and, consequently, lead to a significantly smaller heat-affected zone. This effect increases with higher thermal conductivities of the materials to be joined. For the bonding of FRP/metal joints using weldable inserts it is therefore recommended to select welding parameters that have the lowest possible energy input while preferring short welding times.
2. Small sample width to sheet thickness aspect ratios lead to a larger heat-affected zone when using same welding parameters due to the reduced heat dissipation capacity. Thus, by reducing the outer diameter D of material 1.0338 from 30.0 mm to 25.4 mm at an inner diameter d_3 of 6.8 mm, the isotherm at 149 °C shifts by 0.4 mm towards the peripheral area.
3. For the typical shape of weldable inserts, a reduction of the inner diameter d leads to a shift of the isotherms towards the welding point. This effect increases with smaller inner diameters and is due to the lower heat dissipation capacity in the formed area. As a result of the forming process, a higher dislocation density and a thinning of the material thickness occur locally.
4. The variance of the measured values regarding the radial distance of the isotherms is larger for formed insert geometries compared to plane specimens. To reliably prevent thermal damage to the adjacent fibre composite material in FRP/metal joints, it is therefore appropriate to provide an additional distance of at least 1.0 mm from the welding centre.

Declaration of Competing Interest

The authors declare that there is no conflict of interest regarding the publication of this article.

Funding

This work was financially supported by the Deutsche Forschungsgemeinschaft (German Research Foundation) under project number 418238897.

References

- Akkus, A., 2009. Temperature distribution study in resistance spot welding. *J. Sci. Ind. Res.* 68.
- Bhaves, S., Barbara, F., Caroline, D., Hannes, F., 2010. Structural performance evaluation of composite-to-steel weld bonded joint. In: Proceedings of the Society of Plastics Engineers - 10th Annual Automotive Composites Conference and Exhibition, pp. 545–561.
- Chigurupati, P., Chun, B.K., Bandar, A., Wu, W.T., 2010. Finite element modeling of resistance spot welding process. *Int. J. Mater. Form.* 3 (S1), 991–994.
- Cho, H.S., Cho, Y.J., 1989. A study of the thermal behavior in resistant spot welds: prediction models for temperature distribution and nugget growth compare well with actual spot weld experiments. *Weld. J.* 68 (6), 236–244.
- Chu, T.K., Ho, C.Y., 1978. Thermal conductivity and electrical resistivity of eight selected AISI stainless steels. In: Mirkovich, V.V. (Ed.), *Thermal conductivity 15: Proceedings of the Fifteenth International Conference on Thermal Conductivity*, New York, NY. Plenum Press, pp. 79–104 held in Ottawa, August 24 - 26, 1977.
- Deutsches Institut für Normung e.V., 2004. DIN EN ISO 14327: Widerstandsschweißen-Verfahren für das Bestimmen des Schweißbereichsdiagramms für das Widerstandspunkt-, Buckel- und Rollnahtschweißen (ISO14327:2004);25.160.10(14327). Beuth Verlag GmbH, Berlin.
- Deutsches Institut für Normung e.V., 2015. DIN EN ISO 10447: Widerstandsschweißen - Prüfung Von Schweißverbindungen - Schäl- und Meißelprüfung Von Widerstandspunkt- und Buckelschweißverbindungen;25.160.40(10447). Beuth Verlag GmbH, Berlin.
- Deutsches Institut für Normung e.V., 2010. Widerstandsschweißen: Punktschweiß-Elektrodenkappen;25.160.20(5821). Beuth Verlag GmbH, Berlin.
- Dickinson, D.W., Franklin, J.E., Stanya, A., 1980. Characterization of spot welding behavior by dynamic electrical parameter monitoring. *J. Sci. Ind. Res.* 59, 170–176.
- DIN EN ISO. DIN EN ISO 14373:2015-06, Widerstandsschweißen - Verfahren zum Punktschweißen von Niedriglegierten Stählen mit Oder Ohne Metallischem Überzug (ISO_14373:2015); Deutsche Fassung EN_ISO_14373:2015(14373). Berlin: Beuth Verlag GmbH. 10.31030/2238811.
- DVS/EFB. Fügeverfahren für die Mischbauweise(3451); Düsseldorf; 2016.
- Friedrich, H.E., 2017. Leichtbau in der Fahrzeugtechnik, 2nd ed. Springer Vieweg doi:10.1007/978-3-658-12295-9.
- Gebhardt, J., Schwennen, J., Lorenz, F., Fleischer, J., 2018. Structure optimisation of metallic load introduction elements embedded in CFRP. In: *Prod. Eng.*, pp. 131–140.
- Han, Z., Orozco, J., Indacochea, E., Chen, C.H., 1989. Resistance spot welding: a heat transfer study: real and simulated welds were used to develop a model for predicting temperature distribution. *Weld. J.* 68 (9).
- Hayat, F., 2011. The effects of the welding current on heat input, nugget geometry, and the mechanical and fractural properties of resistance spot welding on Mg/Al dissimilar materials. *Mater. Des.* 32 (4), 2476–2484.
- He, X., 2017. Clenching for sheet materials. *Sci. Technol. Adv. Mater.* 18 (1), 381–405. doi:10.1080/14686996.2017.1320930.
- Holtschke, N., Jüttner, S., 2017. Joining lightweight components by short-time resistance spot welding. *Weld. World* 61 (2), 413–421. doi:10.1007/s40194-016-0398-5.
- Jansen, F., Kunze, A. SoFIA - Structural Organic Sheet Components for the Integration in Automobiles. Bremen; 2016.
- KIM, E.W., Eagar, T.W., 1989. Measurement of transient temperature response during resistance spot welding: high-speed cinematography and infrared emission monitoring are used to evaluate heat transfer with various electrodes. *Weld. J.* 68, 303–312.
- Kocabekir, B., Kaçar, R., Gündüz, S., Hayat, F., 2008. An effect of heat input, weld atmosphere and weld cooling conditions on the resistance spot weldability of 316L austenitic stainless steel. *J. Mater. Process. Technol.* 195 (1–3), 327–335.
- Lehminger, F., Wagner, J., 2015. Challenges in mechanical joining technologies for fibre-reinforced mixed-material car body concepts across the process chain "painted car body". In: *Automotive Circle International, Vincentz Network GmbH & Co. KG, Hannover*, pp. 187–194 Eds. Conference proceedings.
- Lu, Y., Peer, A., Abke, T., Kimchi, M., Zhang, W., 2018. Subcritical heat affected zone softening in hot-stamped boron steel during resistance spot welding. *Mater. Des.* 155, 170–184. doi:10.1016/j.matdes.2018.05.067.
- Meschut, G., Janzen, V., Olfemann, T., 2014. Innovative and highly productive joining technologies for multi-material lightweight car body structures. *J. Mater. Eng. Perform.* 23 (5), 1515–1523. doi:10.1007/s11665-014-0962-3.
- Mirzaei, F., Ghorbani, H., Kolahan, F., 2017. Numerical modeling and optimization of joint strength in resistance spot welding of galvanized steel sheets. *Int. J. Adv. Manuf. Technol.* 92 (9–12), 3489–3501. doi:10.1007/s00170-017-0407-x.
- Moshayedi, H., Sattari-Far, I., 2012. Numerical and experimental study of nugget size growth in resistance spot welding of austenitic stainless steels. *J. Mater. Process. Technol.* 212 (2), 347–354.

- Natarajan, M., Murugavel, S.C., 2017. Thermal stability and thermal degradation kinetics of bio-based epoxy resins derived from cardanol by thermogravimetric analysis. *Polym. Bull.* 74 (8), 3319–3340.
- OMEGA. OMEGALAQ™ Liquid Temperature Lacquers. [June 24, 2018]; Available from: <https://www.omega.de/temperature/pdf/LAQ.pdf>.
- Pepke, L.-A., 2014. Untersuchung Der Anlagenkonfiguration beim Widerstandspunktschweißen von Stahlfeinblechen. Technische Universität Berlin, Berlin.
- Podlesak, F., 2017. Entwicklung und Verifizierung eines Vorlochfreien Mechanischen Fügeverfahrens zum Verbinden von Leichtmetallen und Faser-Kunststoff-Verbunden, 1st ed. Universitätsverlag der TU Chemnitz, Chemnitz.
- Roth, S., Warnck, M., Coutandin, S., Fleischer, J., 2019. RTM process manufacturing of spot-weldable CFRP-metal components. *Lightweight Des. Worldw.* 12 (5), 18–23. doi:10.1007/s41777-019-0046-z.
- Roth, S., Pracisnore, F., Coutandin, S., Fleischer, J., 2020. A new approach for modelling the fibre path in bolted joints of continuous fibre reinforced composites. *Compos. Struct.* 243, 112184. doi:10.1016/j.compstruct.2020.112184.
- Ruffing T., Baron S. Inserts For In-Situ Integration of Assembly Interfaces Into Composite Materials: A Raymond Center of Expertise, Saint-Louis, France. Joining in Car Body Engineering 2019, Detroit, 20.-21.02.2019.
- Schmitt, W.M.A., GmbH B. Schweißparameter: Edelstahl/VA. Ilsfeld-Auenstein; 2015.
- Sheikhi, M., Valaee Tale, M., Usefifar, G.R., Fattah-Alhosseini, A., 2017. Thermal modeling of resistance spot welding and prediction of weld microstructure. *Metall. Mater. Trans. A* 48 (11), 5415–5423. doi:10.1007/s11661-017-4314-4.
- Smithells, C.J., Gale, W.F., Totemeier, T.C., 2004. *Smithells Metals Reference Book*, 8th ed. Elsevier Butterworth-Heinemann, Amsterdam, Boston.
- VDI/VDE, 2015. *Temperature Measurement in Industry: Principles and Special Methods of Temperature Measurement*; 17.200.20(3511). Beuth Verlag GmbH, Berlin.
- Visakh, PM, Araj, Y (Eds.), 2015. *Thermal Degradation of Polymer Blends, Composites, and Nanocomposites* Springer International Publishing AG, Cham, Heidelberg, New York, Dordrecht, London.
- Wan, X., Wang, Y., Zhang, P., 2014. Modelling the effect of welding current on resistance spot welding of DP600 steel. *J. Mater. Process. Technol.* 214 (11), 2723–2729. doi:10.1016/j.jmatprotec.2014.06.009.
- Wilhelm, M., 2016. *Fügarkeit von CFK-Mischverbindungen Mittels Umformtechnischer Prozesse*.
- Zhao, D., Wang, Y., Zhang, P., Liang, D., 2019. Modeling and experimental research on resistance spot welded joints for dual-phase steel. *Mater. Basel* 12 (7). doi:10.3390/ma12071108.